J Intell Robot Syst (2011) 62:3–27
DOI 10.1007/s10846-010-9436-5

Autonomous Shape Control of a Deformable Object by Multiple Manipulators

Jadav Das · Nilanjan Sarkar

Received: 22 July 2009 / Accepted: 7 May 2010 / Published online: 25 May 2010
© Springer Science+Business Media B.V. 2010

Abstract Shape control of a deformable object by a robotic system is a challenging problem because of the difficulty of imposing shape change by a finite number actuation points to an essentially infinite dimensional object. In this paper, a new approach to shape changing of deformable objects by a system of manipulators is presented. First, an integrated dynamic equation of motion for a system of multiple manipulators handling a deformable object is developed. The initial and the final shapes of the deformable object are specified by curves that represent the boundary of the object. We design an optimization-based planner that minimizes an energy-like criterion to determine the locations of the contact points on the desired curve representing the final shape of the object. The motion of each manipulator is controlled independently without any communication between them. Finally we design a robust controller for shape changing that can work in the presence of modeling uncertainty. The simulation results demonstrate the efficacy of the proposed method.

Keywords Deformable object · Multiple manipulators · Shape control · Dynamics

1 Introduction

Deformable objects are used in many economically important industries such as food, automobiles, aerospace, leather and packaging [1–6]. Most of the tasks involving the handling of deformable objects are done manually which make them labor intensive and time consuming requiring fast and accurate manipulation of material by skilled human operators. Automatic handling of rigid objects is readily available (e.g., using multiple robots) and can be reprogrammed to perform different tasks

J. Das (✉) · N. Sarkar
Department of Mechanical Engineering, Vanderbilt University,
Nashville, TN 37205, USA
e-mail: jadav.das@vanderbilt.edu

N. Sarkar
e-mail: nilanjan.sarkar@vanderbilt.edu

when needed [7–9]. Application of such multiple robot systems for handling deformable objects will reduce the time associated with manual handling and increase productivity by lowering the cost and increasing the precision. However, this is a difficult and challenging task primarily due to the low stiffness of the deformable objects that makes them easily susceptible to large deformations. As a result, deformable objects may exhibit deformation by changing in shape and volume under the applied forces during handling. Besides, there are large variations of stiffness and damping properties of different deformable objects which are further influenced by environmental conditions. The aforesaid properties and behavior of deformable objects pose many problems when interacting with robots to automate their handling [4].

Deformable objects are used extensively in a wide range of industrial applications including the manufacturing and assembly of garment and footwear products, the packaging industry and aircraft manufacturing. Manipulation of deformable parts such as inserting an elastic bar into a hole of rigid body and vice versa for precise assembly is a major industrial problem. It can be seen from a survey [4] that although it was identified as a high priority area, very less work has been done on the automated handling of deformable objects. For example, there are real-life applications on food handling where automatic and intelligent handling of deformable objects (e.g., dough-based products) would make the process less labor-intensive and thereby less expensive overall. One of the main problems associated with handling of the deformable object is that the shape of the object can change during manipulation. For example, food products such as fish fillets, jelly block, dough, meat and poultry including sliced hams and other sliced processed meats require delicate handling and packaging because they are often very fragile and easily deformed and spoilt. Also many food products are easily bruised and marked if they are handled with hard/rough surfaces without proper control of contact conditions. Since shape of these food products are linked to their aesthetic values, a bruised or dented donut, for example, will be less attractive to the customers. Therefore, in some cases one would need to achieve some desired shapes of these deformable objects (e.g., inserting a deformable object through a differently shaped hole) while in other cases one may need to preserve the original shape (e.g., preserving the shape of a food product). In either of these situations, the ability of a robotic system to control the shape of the deformable object becomes important. Shape changing task can be found in forming operations of bread dough and pizza dough in food industry and in the formation of clay products of desired shapes in pottery work where a large deformation of the object is required. For instance, the forming process of clay product requires stretching and shrinking operations by multiple fingers. Molding can be used in automatic shape control of deformable objects for batch production. However, there are operations where molding cannot be applied (e.g., pizza dough must be shaped by extending the dough to ensure its quality. Molding the dough decreases the palate of a pizza, [10]) and hence developing an automated process to control the shape of the deformable objects could be beneficial.

In this paper, we address the issue related to shape control of a deformable object by controlling its boundary such that an initial shape is transformed to a desired one. In particular, we focus on the shape control of rheological objects such as dough, clay, tissue etc. which have important applications for automated handling. In this work, we first model a deformable object using a rheological model that

exhibits residual deformation, bouncing displacement and vibration decrease, using an inter-connected mass-spring-damper system. We then discretize the boundary of the deformable object into a set of actuation points such that when these points are actuated by a multiple robotic system, the overall shape of the object will converge to the desired shape. In general, the more the number of actuation points distributed over the boundary, the better will be the performance in controlling the shape change. How many actuation points are necessary to effect a desired shape change and where these points should be located on the boundary of the deformable object are open questions that will depend on the shape of the object and the nature of the desired deformation and are not addressed here. In this paper, we focus on the problem of effecting shape change on a deformable object given the initial actuation points. That is, we design a controller for deforming the object from an initial shape to a final one if we know how many actuation points are available and where they are located. Also note that the nature and capabilities of the end-effectors of the manipulators are important for effecting shape change. For example, the nature of shape control will be different if the end-effector can only apply push or pull or both to deform the object. We then develop the coupled dynamics of the multiple manipulators along with the deformable object. We develop a control law for shape changing based on the inverse dynamics method. We design a planner based on an optimization technique to compute the desired final contact locations. The performance of a controller that requires an exact model may not be useful in real-world situation. Therefore, we introduce robustness into the controller for shape changing that can work in the presence of modeling uncertainty. We show the efficacy of the method using extensive computer simulations.

The remainder of this paper is organized as follows: in Section 2, we discuss the existing literature on deformable object modeling and shape control. A mathematical description of the problem is given in Section 3. Section 4 outlines the procedure to derive the mathematical model of the deformable object. We also develop the integrated dynamics involving the object dynamics and the manipulator dynamics, and the control method in this section. The effectiveness of the derived control law is demonstrated by simulation in Section 5. Finally, the contributions of this work and the future directions are discussed in Section 6.

2 Existing Literature on Deformable Object Modelling and Shape Control

A considerable amount of work has been performed on multiple robotic systems during the last few decades [7–9, 11–21]. Mostly, the position and/or force control of multiple manipulators handling a rigid object were studied in [7–9]. However, there were some works on handling deformable object by multiple manipulators presented in [11–21]. Saha and Isto [11] presented a motion planner for manipulating deformable linear objects using two cooperating robotic arms to tie self-knots and knots around simple static objects. Zhang et al. [12] presented a microrobotic system that is capable of picking up and releasing operation of microobjects. The system is capable of rapid contact detection and reliable force-controlled (PID) for micrograsping of interstitial cells to accommodate variations in size [13, 14]. Petterson et al. [15] developed a robot gripper using the effects of a magnetorheological fluid for handling natural food products with varying shapes. In [16], Tavasoli et al.

presented two-time scale control design for trajectory tracking of two cooperating planar rigid robots moving a flexible beam. Tanner et al. [17] developed a system of multiple mobile manipulators that handle a deformable object during an agricultural task. Sun et al. [18] presented a cooperation task of controlling the reference motion and the deformation when handling a deformable object by two manipulators. In [19] the control of position/orientation and the vibration suppression of each contact points of a flexible object by two manipulators were presented. Liu and Nakamura [20] studied the assembly operation of inserting a flexible beam into a rigid hole. Hirai et al. [21] developed a robust control law for manipulation of 2D deformable parts using tactile and vision feedback to control the motion of the deformable object with respect to the position of selected reference points. However, to the best of our knowledge there is no such work on controlling the overall shape of a deformable object by multiple manipulators.

A wide variety of modeling approaches have been presented in the literature dealing with computer simulation of deformable objects [22]. These are mainly derived from physically-based models to produce physically valid behaviors. Mass-spring models are one of the most common forms of deformable objects. A general mass-spring model consists of a set of point masses connected to its neighbors by massless springs. Mass-spring models have been used extensively in facial animation [23], cloth motion [24] and surgical simulation [25]. Tokumoto et al. [10] proposed a modeling method of viscoelastic objects for deformation control. They used a lattice structure to describe deformation of a viscoelastic object in 3D space. A four element model consisted of a series of a Voigt model and a Maxwell model was used. Many researchers have used finite element methods to model the deformable objects. Finite element models have been used in the computer simulation to model facial tissue and predict surgical outcomes [26, 27]. Keeve et al. [28] compared mass-spring and FEM models for maxillofacial surgery. Their comparison was based on a qualitative visual inspection of the predicted facial outlooks calculated with each model. They concluded that although the mass-spring model could never be exact, the speed and the easy architecture of this model could be a serious advantage over the more accurate but computationally intensive finite element model. An important issue of modeling deformable objects such as food (e.g., dough) and tissue (e.g., organs) is that they have both elasticity and viscosity properties. These objects are called rheological objects. A comprehensive study on rheological objects based on three main deformation properties such as residual deformation, bouncing displacement and vibration decrease was performed by Kimura et al. [29]. It is concluded that a three element model i.e., a spring and a damper in parallel (Voigt model) with another damping element in series gives an appropriate choice of deformable object modeling, which we choose in this work.

Considerable effort has been put into the design of robust and optimal control methods for shape control of 2-D flexible structure. Various approaches for shape control algorithm were presented in [5, 30–32]. A robust shape control of a flexible structure against parameter variation was presented in [30]. Kashiwase et al. [31] proposed a simple zero P-ID controller by using many sensors and actuators. Dang et al. [32] developed a shape control algorithm of a flexible structure that is used for shape morphing. These works are important and have many useful applications such as morphing of aircraft wings. In all of these cases, microactuators are used for shape morphing of flexible structures that are embedded or bonded on the

surface. Thus these works focus on small deformation (i.e., micro actuation) and are not geared towards producing macro-level shape change of the object. In our intended application, for example changing the shape of a dough, we will need large deformation. Another difference between the above works and ours is in the manner in which shape change occurs. We present a technique to effect the shape change by actuating the boundary of the deformable objects; whereas the micro actuation works embed the actuators within the whole surface of the body. It is not possible to embed micro actuators in our intended application domain. Also note that, in our framework, it is possible to apply pulling, pushing, stretching etc. at the boundary contact points to create the intended shape. There are a few other works that are worth mentioning in this context. Hirai et al. [21] proposed a control law for the positioning of multiple points of extensible cloths using robotic actuators. However, the shape of the cloth is not controlled.

In other areas, various methods have been presented in computer graphics to represent shapes of curved lines and curved surfaces [22]. Shape of cloths [24], animation of deformable characters [33], virtual sculpting [34] and shape of elastic objects [35] have also been studied. These are computer graphics works that consider virtual elastic objects. These are not applicable to shape changing operation of deformable rheological objects directly since they mainly focused on deformed shapes of objects and manipulation process are not formulated there. In our work, we model the deformable object with physics based mass-spring-damper system to represent the shape of the object. We formulated a manipulation technique to apply push, pull on the surface of the deformable object to deform it to a desired shape. Note that in our application, we consider the dynamics of the robot that applies these forces, whereas in the computer graphics applications the dynamics of actuations is not modeled.

In the area of robotic grasping, various robotic grippers have been developed for manipulating deformable objects such as microgripper for manipulating microobjects [12], endoscopic surgical grasper [36], reconfigurable robotic gripper [37], end-effector to handle bulk material such as meat, dough [38] and Cryo gripper for handling fabrics [39]. However, the shape control of the deformable object is not attempted during these applications. In our work, it is possible to control the shape of the deformable object while simultaneously manipulating the object.

It is always important to measure the similarity between the final and the desired shapes of the object. To measure similarity, various techniques have been developed in the past few decades using the image data [40, 41]. These are useful to group similar shapes together and separate dissimilar shapes into different groups. Fourier descriptor [42], wavelet descriptor [43], Hough transform [44], geometric hashing [45], deformable template [46], relaxation labeling [47], curvature scale space [48], and neural network [49] are used mostly for shape representation and description. In this work, we use an area descriptor [40] to measure the dissimilarity between the final and the desired shapes of the object.

3 Problem Statement

Consider a planar deformable object that moves and changes in time defining a new shape when subjected to applied forces. We define that the object is a compact

and closed set in $\Re^2$. The boundary of such a set is represented by a closed two dimensional curve. This closed curve is described parametrically as

$$\mathbf{c}(\sigma) = \big[x(\sigma),\, y(\sigma)\big]^T \tag{1}$$

where, σ is the normalized curve parameter, $0 \leq \sigma \leq 1$. For example, the boundary of a circular section of a deformable object can be represented as $\mathbf{c}(\sigma) = [r\cos(2\pi\sigma), r\sin(2\pi\sigma)]$, where r is the radius and σ is the normalized curve parameter varying [0, 1].

The motion of a deformable object can be described by translation, rotation and deformation. Translation and rotation can be described by the translation of the center of mass of the object and a rotation about an axis passing through the center of mass, while the deformation can be analyzed by the dynamics of shape change.

Thus, the shape error can be defined as

$$D = \sum_{k=1}^{\infty} \big\|\mathbf{c}(\sigma_k) - \hat{\mathbf{c}}(\sigma_k)\big\| \tag{2}$$

where, $\mathbf{c}(\sigma)$ is the actual shape and $\hat{\mathbf{c}}(\sigma)$ is the desired shape. In this paper, we investigate the shape change problem in the following form:

Problem: Given a desired shape $\hat{\mathbf{c}}(\sigma)$ and a current shape $\mathbf{c}(\sigma)$ of the planar object, find a control action on $\mathbf{c}(\sigma)$, such that the shape error $D(\mathbf{c}(\sigma), \hat{\mathbf{c}}(\sigma))$ defined according to some norm is minimum.

It is reasonable to pose the above problem of controlling the shape of a deformable object by controlling its boundary. However, since the boundary of the object, i.e., the current shape will be actuated by a finite number of actuation points, say n, the above problem is restated as follows:

Define all end effectors positions that are also the contact points on the deformable objects $\mathbf{p}(\mathbf{q}) \in \Re^{2n}$ as

$$\mathbf{p}(\mathbf{q}) = \begin{bmatrix} \mathbf{p}_1(\mathbf{q}) \\ \vdots \\ \mathbf{p}_n(\mathbf{q}) \end{bmatrix} \tag{3}$$

where, $\mathbf{q}$ is the joint variable of the manipulators. Define also the location of these contact points on the desired curve $\mathbf{p}_d(\boldsymbol{\sigma}) \in \Re^{2n}$ as

$$\mathbf{p}_d(\boldsymbol{\sigma}) = \begin{bmatrix} \hat{\mathbf{c}}(\sigma_1) \\ \vdots \\ \hat{\mathbf{c}}(\sigma_n) \end{bmatrix} \tag{4}$$

where, $\sigma_i \in \Re (i = 1, \ldots, n)$ is a curve parameter corresponding to the position of the i-th manipulator. Then define the shape error at the actuation points, $\mathbf{e}(\mathbf{q}, \boldsymbol{\sigma}) \in \Re^{2n}$, as

$$\mathbf{e}(\mathbf{q}, \boldsymbol{\sigma}) = \mathbf{p}(\mathbf{q}) - \mathbf{p}_d(\boldsymbol{\sigma}) \tag{5}$$

The overall shape error of the object is defined as the summation of the shape error at each actuation point expressed as

$$d = \sum_{i=1}^{n} \left\| \mathbf{e}_i(\mathbf{q}_i, \sigma_i) \right\| \tag{6}$$

Note that the above definition of the shape error assumes the discrepancy in each contact point location between the initial shape and the final desired shape. It is a discrete representation of the shape error. Thus a controller that reduces this error to zero does not guarantee that all points on the curve will exactly match the desired curve. However, it will be shown in Section 5 that such discrete definition, which is motivated by practicality (e.g., a limited number of actuation points), produce acceptable shape change results. It will also be shown that as the number of contact points increases, the convergence to the desired shape improves.

Thus the problem becomes Given a desired shape and a current shape of the planar object, and also given the number of actuation points, find a control action such that $\mathbf{e}(\mathbf{q}, \boldsymbol{\sigma}) \rightarrow \mathbf{0}$.

4 Modeling of System Dynamics

Consider a schematic in Fig. 1 where n manipulators are performing a cooperative task on a deformable object changing shapes from $\mathbf{c}(\sigma)$ to $\hat{\mathbf{c}}(\sigma)$. We assume that all the manipulator grippers are firmly attached to the deformable body such that the end-effectors can apply both push and pull on the object as needed. Knowing the positions of the manipulator tips at the moment when the contact with the manipulated object is made, we derive the mathematical model of the whole system such that all the manipulators can induce the desired motion.

The coordinate systems are defined as follows: Σ_w is the task coordinate system, Σ_o is the object coordinate system, fixed on the object and Σ_i is the i-th manipulator coordinate system, fixed on the i-th end-effectors located at the grasping point. We

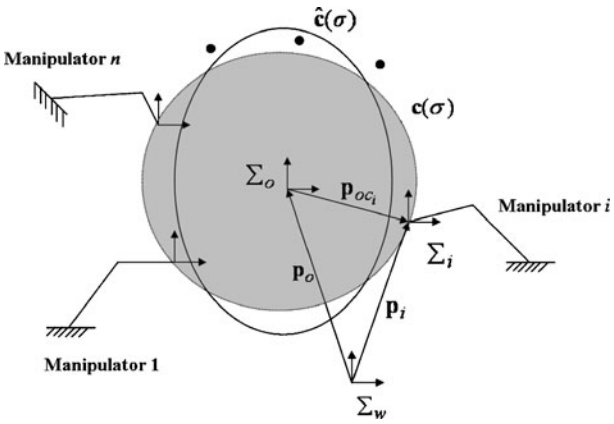

Fig. 1 Schematic of manipulators handling a deformable object

also define $\mathbf{p}_0 \in \Re^2$ is the position vector of the origin of the object coordinate system Σ_o with respect to Σ_w, $\mathbf{p}_i \in \Re^2$ is the position vector of the origin of Σ_i with respect to Σ_w, $\mathbf{p}_{oc_i} \in \Re^2$ is the position vector from the origin of Σ_o to the origin of Σ_i with respect to Σ_w.

4.1 Deformable Object Dynamics

We model the deformable body as a rheological object using discrete networks of mass-spring-damper system similar to [29]. The mass points are located at the nodal points and a three element model is inserted between the neighboring mass points. Figure 2 shows a single layer of the deformable object. Each element is labeled as E_j for $j = 1, 2, \ldots, NE$, where NE is total number of elements in a single layer. We consider that each mass point in the mesh is having two degrees of freedom consisted of two translational motions in x-and y-direction.

Let us formulate the behavior of three element model as shown in Fig. 2. Let $\mathbf{z}_i$ and $\mathbf{z}_j$ be two end points of a three element model. Elastic and viscosity coefficients of the non-residual deformation part (Voigt model) are denoted as k_1 and c_1, respectively. The viscosity coefficient in the residual deformation part is denoted as c_2. The natural length of the non-residual deformation part is given by L_1, and the natural length of the residual deformation part is given by L_2. Let $\mathbf{z}_i^1$ be the point at the junction between non-residual and residual deformation parts. Since the points $\mathbf{z}_i$, $\mathbf{z}_i^1$ and $\mathbf{z}_j$ lie on a straight line, the position of point $\mathbf{z}_i^1$ can be defined by a parameter α as $\mathbf{z}_i^1 = \alpha(\mathbf{z}_j - \mathbf{z}_i) + \mathbf{z}_i$. The time varying unit direction vector along $\overrightarrow{\mathbf{z}_i\mathbf{z}_j}$ is defined as $\mathbf{e}_{ij} = (\mathbf{z}_j - \mathbf{z}_i)/\|\mathbf{z}_j - \mathbf{z}_i\|$ and also time varying length coefficient is defined as $R_1 = \alpha\|\mathbf{z}_j - \mathbf{z}_i\|$. The length of the residual deformation part is given by $R_2 = \|\mathbf{z}_j - \mathbf{z}_i\| - R_1$. Let $\mathbf{f}_{ij}$ be a force at point $\mathbf{z}_i$ exerted by an element between points $\mathbf{z}_i$ and $\mathbf{z}_j$. The force $\mathbf{f}_{ij}$ equals to force acting on the non-residual deformation part, that is,

$$\mathbf{f}_{ij} = -c_1 \dot{R}_1 \mathbf{e}_{ij} - k_1(R_1 - L_1)\mathbf{e}_{ij} \tag{7}$$

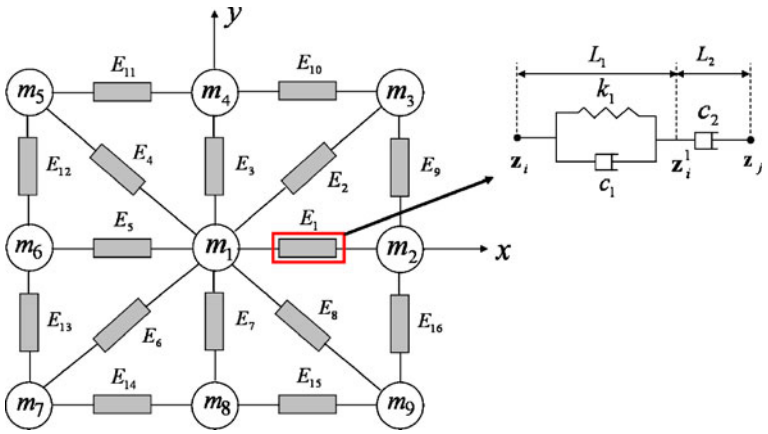

Fig. 2 Model of a rheological object with interconnected mass-spring-damper

Also, the force $\mathbf{f}_{ij}$ coincides with the force caused by damper of residual deformation part, that is,

$$\mathbf{f}_{ij} = -c_2 \dot{R}_2 \mathbf{e}_{ij} \tag{8}$$

Equating Eqs. 7 and 8, we can determine parameter α uniquely. Substituting the value of α, we can determine the value of $\mathbf{f}_{ij}$.

Let m_i be the mass point at the i-th node of the system. The dynamic equation representing each mass point can be written in the standard form as,

$$\mathbf{M}_{oi}\ddot{\mathbf{z}}_i + \mathbf{C}_{oi}\dot{\mathbf{z}}_i + \mathbf{G}_{oi} = \mathbf{F}_i + \mathbf{F}_i^{\text{int}} \tag{9}$$

for $i = 1, 2, \ldots, N$ where N is the total number of mass points in a layer. $\mathbf{z}_i \in \Re^2$ is the position vector at the i-th mass point represented as $\mathbf{z}_i = [x_i, y_i]^T$, $\mathbf{M}_{oi} \in \Re^{2\times 2}$ is the symmetric positive definite mass matrix, $\mathbf{C}_{oi} \in \Re^{2\times 2}$ is the coriolis matrix, $\mathbf{G}_{oi} \in \Re^2$ is denoted the terms containing stiffness, spring lengths etc., $\mathbf{F}_i \in \Re^2$ is the external force vector given by $\mathbf{F}_i = [F_{ix}, F_{iy}]^T$ acting on mass point $\mathbf{z}_i$. In this paper, $\mathbf{F}_i$ represents the contact force exerted by the manipulators. $\mathbf{F}_i^{\text{int}} \in \Re^2$ is the internal reaction force vector generated due to the interaction among the mass points in the network.

4.2 Manipulator Dynamics

Consider n planar manipulators with 2 DOF are handling a deformable object on the plane. The Lagrange equation of motion of the i-th manipulator in the Cartesian space is given by

$$\mathbf{M}_i(\mathbf{q}_i)\ddot{\mathbf{p}}_i + \mathbf{C}_i(\mathbf{q}_i, \dot{\mathbf{q}}_i)\dot{\mathbf{p}}_i + \mathbf{G}_i(\mathbf{q}_i) = \mathbf{u}_i - \mathbf{F}_i \tag{10}$$

where $\mathbf{q}_i \in \Re^2$ is the joint variables, $\mathbf{p}_i \in \Re^2$ is the position vector of the i-th end-effector, $\mathbf{M}_i(\mathbf{q}_i) \in \Re^{2\times 2}$ denotes the symmetric positive definite inertia matrix, $\mathbf{C}_i(\mathbf{q}_i, \dot{\mathbf{q}}_i) \in \Re^{2\times 2}$ accounts for the coriolis effects, $\mathbf{G}_i(\mathbf{q}_i) \in \Re^2$ represents the elastic effects due to spring and bending stiffness. $\mathbf{u}_i \in \Re^2$ is the control input and $\mathbf{F}_i \in \Re^2$ is the contact force that the end-effectors exerts on the object.

4.3 Coupled Dynamics of Multiple Manipulators and a Deformable Object

In order to integrate the dynamics of the multiple manipulators with the dynamics of the deformable object, we first rewrite the dynamics of the deformable objects in terms of two classes of mass points, one set represents the n number of mass points that are in contact with the manipulators and the rest of the mass points (i.e., $N - n$) that constitute the object model. The dynamics of the first set of mass points are written by replacing $\mathbf{z}$ by $\mathbf{p}$ as

$$\mathbf{M}_{oi}\ddot{\mathbf{p}}_i + \mathbf{C}_{oi}\dot{\mathbf{p}}_i + \mathbf{G}_{oi} = \mathbf{F}_i + \mathbf{F}_i^{\text{int}}, \quad i = 1, 2, 3, ..., n \tag{11}$$

And the second set of dynamics equations are written as

$$\mathbf{M}_{oj}\ddot{\mathbf{z}}_j + \mathbf{C}_{oj}\dot{\mathbf{z}}_j + \mathbf{G}_{oj} = \mathbf{F}_j^{\text{int}}, \quad j = n + 1, ..., N \tag{12}$$

By eliminating $\mathbf{F}_i$ from the manipulator dynamics (10) and the object dynamics of the first set (11), the coupled dynamics between the manipulators and the contact mass points are obtained as follows:

$$\overline{\mathbf{M}}_i\ddot{\mathbf{p}}_i + \overline{\mathbf{C}}_i\dot{\mathbf{p}}_i + \overline{\mathbf{G}}_i = \mathbf{u}_i \tag{13}$$

where, $\overline{\mathbf{M}}_i = \mathbf{M}_i + \mathbf{M}_{oi}$, $\overline{\mathbf{C}}_i = \mathbf{C}_i + \mathbf{C}_{oi}$, and $\overline{\mathbf{G}}_i = \mathbf{G}_i + \mathbf{G}_{oi} - \mathbf{F}_i^{\text{int}}$

The coupled dynamics can be rewritten more concisely for all contact mass points as follows:

$$\overline{\mathbf{M}}\ddot{\mathbf{p}} + \overline{\mathbf{C}}\dot{\mathbf{p}} + \overline{\mathbf{G}} = \mathbf{u} \tag{14}$$

where, $\mathbf{p} = \left(\mathbf{p}_1^T \cdots \mathbf{p}_n^T\right)^T$, $\overline{\mathbf{M}} = blockdiag(\overline{\mathbf{M}}_1 \cdots \overline{\mathbf{M}}_n)$, $\overline{\mathbf{C}} = blockdiag(\overline{\mathbf{C}}_1 \cdots \overline{\mathbf{C}}_n)$, $\overline{\mathbf{G}} = \left(\overline{\mathbf{G}}_1^T \cdots \overline{\mathbf{G}}_n^T\right)^T$, and $\mathbf{u} = \left(\mathbf{u}_1^T \ldots \mathbf{u}_n^T\right)^T$.

Equation 14 can be used to design the control law for the manipulators and Eq. 12 can be integrated to find the position of the internal mass points and the boundary mass points those are not interacted by the manipulators. The motion of these mass points are affected by the reaction forces generated due to the interaction.

4.4 Design of the Shape Controller

We develop a new approach to control the shape of a deformable object. We design an optimization technique to find the desired curve parameters that are used as reference contact locations for the controller. In this context, we define an energy-like criterion based on the shape error between the desired and the initial shapes of the object. As we are actuating a finite number of points on the initial object to deform it to the desired final shape, we need to find out the final locations of the initial contacts. Therefore, we define an error between the initial contact points and the boundary curve of the desired object as $\varepsilon_i(\boldsymbol{\sigma}) = \mathbf{p}_i(\mathbf{q}) - \mathbf{p}_d(\boldsymbol{\sigma}), i = 1, 2, \ldots, n$. The energy required for deformation of each contact point can be calculated and then the total energy will be the summation of energies of all contacts location as discussed below. Minimization of the total energy will give the optimal location of the initial contact points used as reference contact locations for the controller.

The energy-like function is given by :

$$\boldsymbol{\Pi} = \sum_{i=1}^{n} \varepsilon_i(\boldsymbol{\sigma})^T \mathbf{W}_i \varepsilon_i(\boldsymbol{\sigma}) \tag{15}$$

where $\mathbf{W}_i \in \Re^{2\times 2}$ are diagonal weight matrices. The optimal values of the curve parameters will be the solution of the unconstrained optimization problem:

$$\min_{\sigma_i \in \boldsymbol{\sigma}} \boldsymbol{\Pi} \tag{16}$$

We get n algebraic equations by differentiating Eq. 15 with respect to $\sigma_i (i = 1, \ldots, n)$ as

$$\frac{\partial \Pi}{\partial \sigma_i} = 0 \ (i = 1, \cdots, n) \tag{17}$$

The solution of Eq. 17 provides the optimal values of σ_i.

To clarify the process of how the desired contact locations are calculated, we take a case of transforming a circle into an ellipse as shown in Fig. 3. The equation of

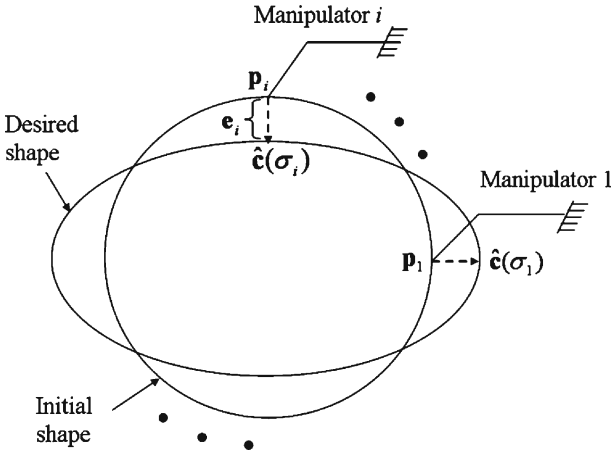

Fig. 3 Manipulators with the initial and the desired shapes of the object

the ellipse is given by $\hat{\mathbf{c}}(\sigma) = [a\cos(2\pi\sigma), b\sin(2\pi\sigma)]$, where a and b are the lengths of the major and minor axis, respectively, and σ is the curve parameter. Knowing the initial contact locations of all the manipulators, $\mathbf{p}_i$, we can find the desired curve parameter, σ_i from Eq. 17. Hence, we obtain the desired x and y coordinates on the desired curve by inserting the σ_i values in the parametric representation of the ellipse.

After getting the desired curve parameters, the planner generates the desired reference locations for the chosen contact points. All manipulators in the system are controlled to execute the desired motion at the contact points of the object such that the initial contact points converge to the desired contact points as obtained from optimization in a planned manner using the following control law

$$\mathbf{u} = \overline{\mathbf{M}}\mathbf{v} + \overline{\mathbf{C}}\dot{\mathbf{p}} + \overline{\mathbf{G}} \tag{18}$$

$$\mathbf{v} = \mathbf{J}_{\mathbf{M}}^{-1}\left\{\ddot{\mathbf{p}}_d - \dot{\mathbf{J}}_{\mathbf{M}}\dot{\mathbf{q}} - \mathbf{K}_p\mathbf{e} - \mathbf{K}_d\dot{\mathbf{e}}\right\} \tag{19}$$

where, $\mathbf{J}_{\mathbf{M}} \in \Re^{2n\times 2n}$ is the Jacobian of the manipulator, and $\mathbf{K}_p$, and $\mathbf{K}_d \in \Re^{2n\times 2n}$ are symmetric and positive definite matrices, and $\ddot{\mathbf{p}}_d \in \Re^{2n}$is desired acceleration which is zero in our present case as we assume that the final contact locations for each manipulators are constant in the time of interest.

Substituting the control law (18) and (19), into the integrated system (14), we obtain the following error system.

$$\ddot{\mathbf{e}} + \mathbf{K}_d\dot{\mathbf{e}} + \mathbf{K}_p\mathbf{e} = 0 \tag{20}$$

which shows that $\mathbf{e}$ and $\dot{\mathbf{e}}$ converge to zero exponentially when $\mathbf{K}_p$, and $\mathbf{K}_d$ are symmetric and positive definite.

The performance of the control action can be improved if we do the optimization in each time-step to find the next desired contact locations. This may be needed when the model is not exact. However, implementation of dynamic optimization in each time-step is computationally intensive. To overcome this problem we augment the controller in Eq. 18 to perform robustly in the presence of modeling uncertainty by

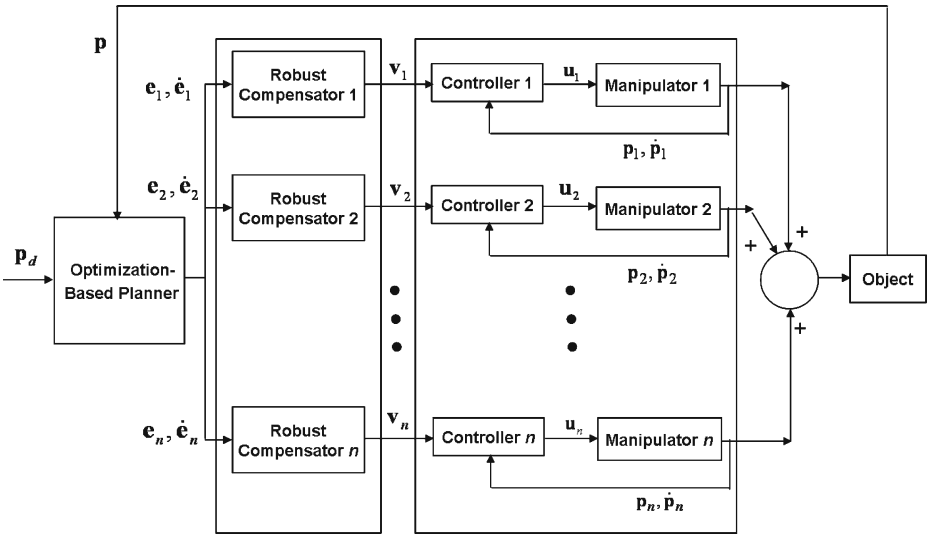

Fig. 4 Schematic of the proposed controller

designing a robust outer loop, which is discussed in the "Appendix". The schematic of the proposed controller is shown in Fig. 4.

5 Simulation and Discussion

We present two sets of simulations to demonstrate the efficacy of the proposed shape controller. The first set consists of applications of the shape controller to deform an initial shape to a final desired shape, which can occur in various applications such as clay modeling, food processing etc. In the second set of simulations, we use the shape controller to preserve the shape of a deformable object while manipulating it. Such a situation may occur in handling food products.

Simulation Set 1: In this section, we present two shape control tasks by multiple manipulators using the developed control laws. We choose a circular deformable object of diameter 0.08 m as the initial shape of the object. The goal is to deform it to obtain two different shapes: i) an ellipse, and ii) a square. The desired shapes can be represented as:

1. For the ellipse, $\hat{\mathbf{c}}(\sigma) = [a\cos(2\pi\sigma), b\sin(2\pi\sigma)]$, where $a = 0.05$ m, $b = 0.032$ m, and $\sigma \in [0\ 1]$.
2. For the square, the vertices are $[(a, 0), (0, a), (-a, 0), (0, -a)]$, where, $a = 0.05$ m. In this work, we represent the square using a B-spline to get a continuous representation of the boundary.

We discretize the circle with 145 elements of mass-spring-damper and a few elements are shown in Fig. 5. We assume that the total mass remains constant during the whole deformation process. Referring to [50] for a rheological object model of wheat dough we take $m = 0.006$ kg for each point mass, $k_1 = 460$ N/m for the spring

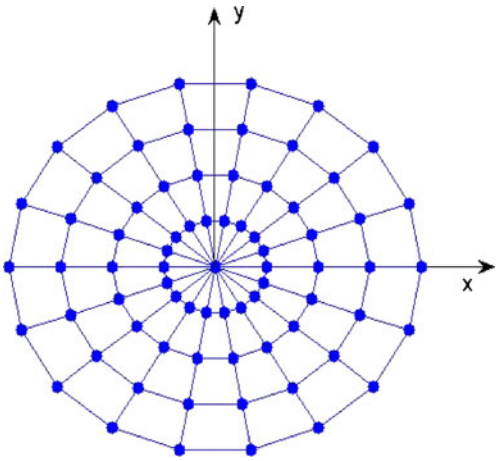

Fig. 5 Deformable object with discretized points

constant and $c_1 = 2452$ Ns/m for the damping coefficient of non-residual deformation part. The damping coefficient of the residual deformation part is taken as $c_2 = 4904$ Ns/m. In this simulation, we use $\mathbf{K}_p = k_p\mathbf{I}$, and $\mathbf{K}_d = k_d\mathbf{I}$ where $k_p = 500$, $k_d = 50$ and $I \in \Re^{2\times 2}$ unity matrix. We present four different simulations based on the number of actuation points placed on the periphery of the object. Note that each actuation point is the result of one manipulator contacting the object. In particular, we choose 12, 18, 24, and 36 actuation points placed equidistantly in all cases as our initial contact locations. The tasks are presented below:

Task 1: In Task 1, the optimization-based planner (Eq. 16) is used to determine the desired final contact locations of the initial contact points, which are then given to the controller (Eq. 18) as the reference final locations to be achieved. The desired final contact locations for 36 contacts points on the pheripery of the object along with their initial contact locations are shown in Fig. 6. Initial contact locations are denoted

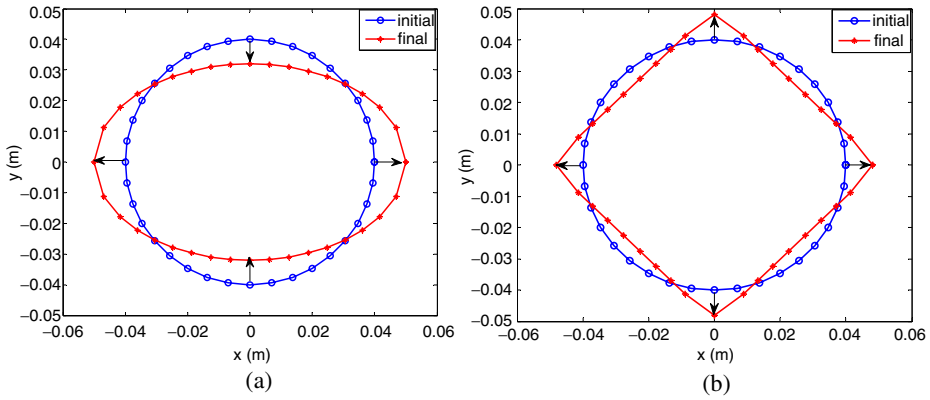

Fig. 6 The initial (*blue circle*) and the final desired (*red asterisk*) contact locations on the boundary of the initial and final objects when (**a**) the *circle* is deformed to the *ellipse* and (**b**) the *circle* is deformed to the *square*

by circle on the undeformed object and their corresponding desired final locations are denoted by asterisk on the final object. The planner sends those reference final locations to each controller and the end-effector of each manipulator follows the reference independently without any communication between them. The initial, the desired and the final shapes of the deformable object when controlling shape from the circle to the ellipse and from the circle to the square are shown in Figs. 7 and 8. In these figures we are showing only the boundary points to represent the shapes. These figures show the feasibility of obtaining the desired shapes by using the presented control law. As expected, the performance increases with increasing the number of contact points. The time responses of the root mean square (RMS) of the shape error at the actuation points, **e**, are depicted in Figs. 9 and 10. The figures show their convergence to zero. The overall shape of the object is dictated by the points located at the boundary. Some of them are actuated by the manipulators to their corresponding desired locations and some of them are not but their motions are predicted dynamically due to the reaction forces among the neighboring mass points. As the actuation points reach to their desired locations it is expected that the points those are not actuated take the shape of the desired object within an acceptable limit due to the rheological nature of the object. If we increase the number of actuation

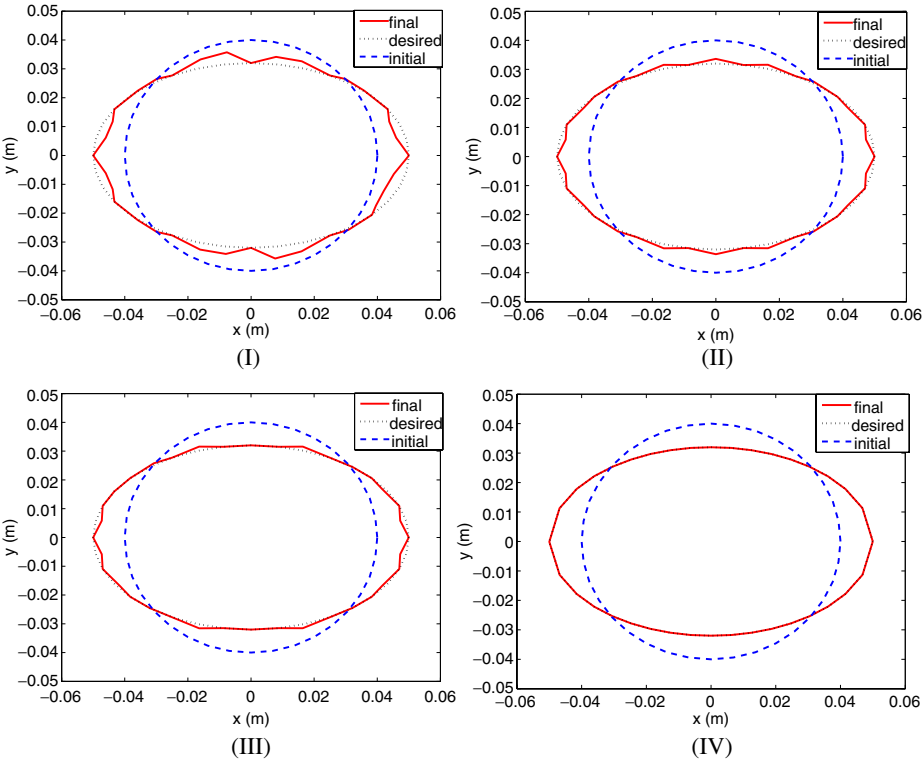

Fig. 7 Initial (*blue dashed*), desired (*black dotted*) and final (*red solid*) shapes for four different cases based on number of actuation points when controlling shape from the *circle* to the *ellipse*: (I) 12, (II) 18, (III) 24, and (IV) 36

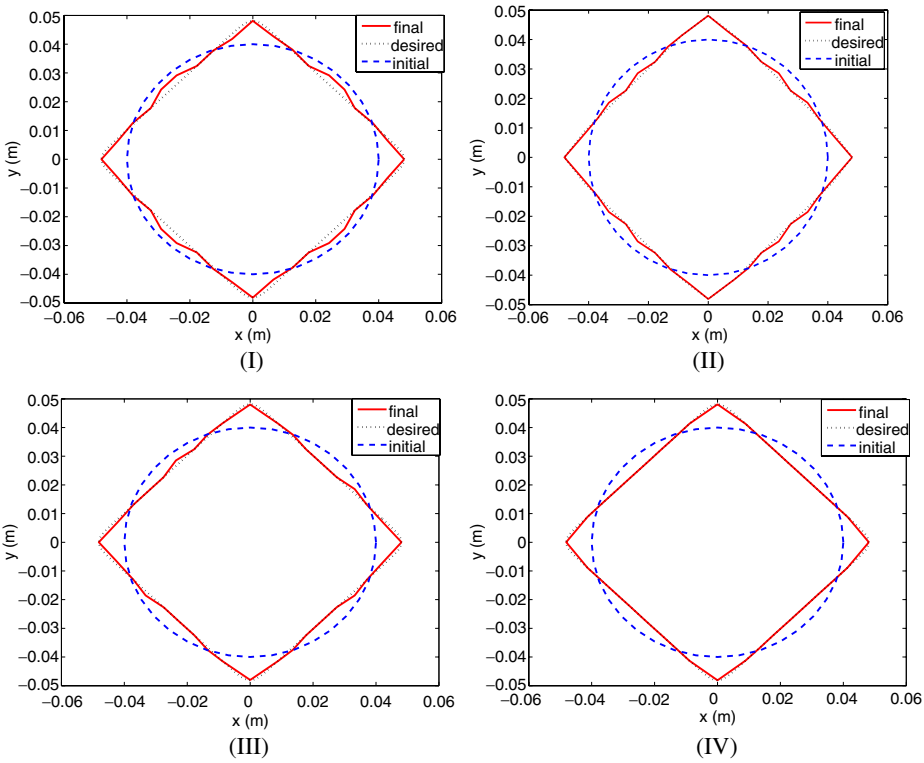

Fig. 8 Initial (*blue dashed*), desired (*black dotted*) and final (*red solid*) shapes for four different cases based on number of actuation points when controlling shape from the *circle* to the *square*: (I) 12, (II) 18, (III) 24, and (IV) 36

points the accuracy improves. To this end we calculate the area enclosed by the shape achieved due to the finite number of actuation to measure the dissimilarity with the desired shape. The boundaries of the desired objects are represented by continuous curves and their exact areas are calculated as 0.005 m^2. The absolute difference between the actual and desired areas gives the dissimilarity measure shown in Fig. 11. These figures show that as we increase the number of actuation points the dissimilarity decreases. Take a particular case of 18 actuation points where there is a finite amount of dissimilarity present in the final shape although the RMS of shape error at the actuation points is zero (shown in Figs. 7(II) and 9(II) when controlling shape from the circle to the ellipse and **8(II)** and **10(II)** when controlling shape from the circle to the square). This dissimilarity is finite and bounded. Hence, we can show that the final shape of the object is stable. The forces exerted on the object to change the shape from the circle to the ellipse and from the circle to the square are shown in Figs. 12 and 13 for case IV of three different contact locations. It can be seen that the forces are high initially and decrease with time as the shapes converge to the desired one. Forces of all other contact points also reduce with time when the shape converges to the desired one. Force values reach to zeros when final shapes are achieved.

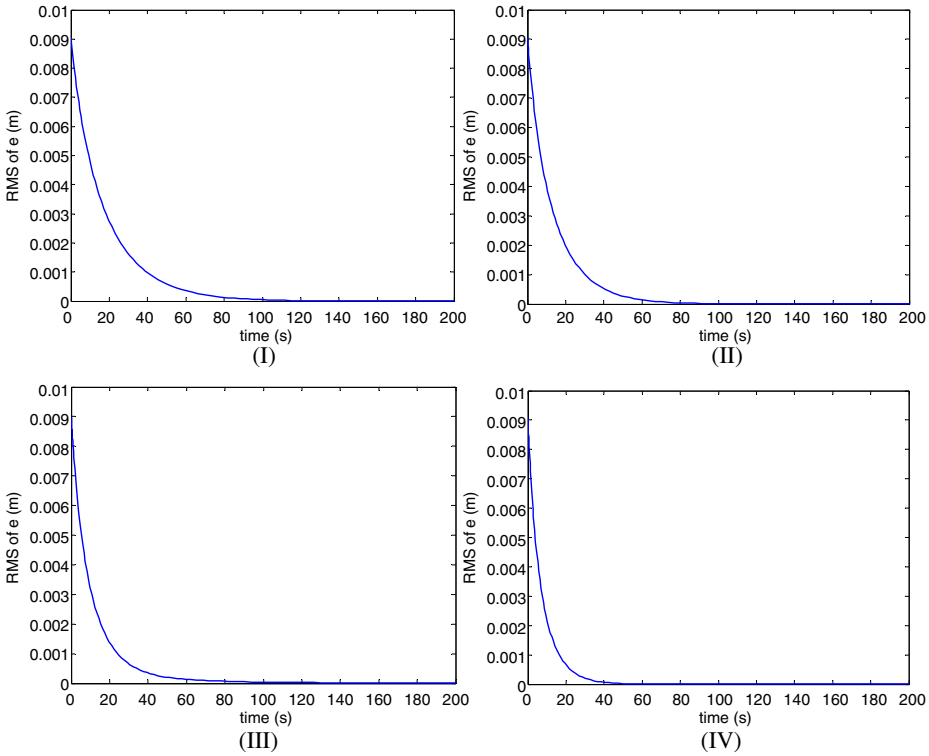

Fig. 9 RMS of shape error, e, for four different cases based on number of actuation points when controlling shape from the *circle* to the *ellipse*: (I) 12, (II) 18, (III) 24, and (IV) 36

Task 2: In Task 2, the control system robustness of the deformable object with parameter uncertainty is presented. The uncertainty includes the changes of the parameters values that are greatly affected by small changes in temperature and humidity, etc. To demonstrate the performance of the shape controller, two simulations are conducted, (i) the system model contains parameter uncertainties but the controller does not consider them, and (ii) the robust control method is used to control the system with parameter model uncertainties. For this case, we increase the parameters m, k_1, and c_1 by 25% and take $c_2 = 9000$ Ns/m with the same controller gains as before. The controller described by Eq. 18 is used without consideration of the additional control term due to the presence of model parameter uncertainty. The time responses of the RMS of shape error at the actuation points when controlling shape from the circle to the ellipse and from the circle to the square with 36 contact points are shown in Figs. 14a and 15a. It is noticed that the convergence of shape error is slow and it is not converged to zero up to 200 s of simulation run. The presence of modeling uncertainty affects the speed of convergence during handling. Therefore, to maintain or speed up the efficiency of shape changing the error should be suppressed during the motion. In the second case, the robust shape control described by Eq. 21 is used to control the shape of the deformable object with the presence of modeling uncertainty. The time responses of RMS of shape error are shown in Figs. 14b and

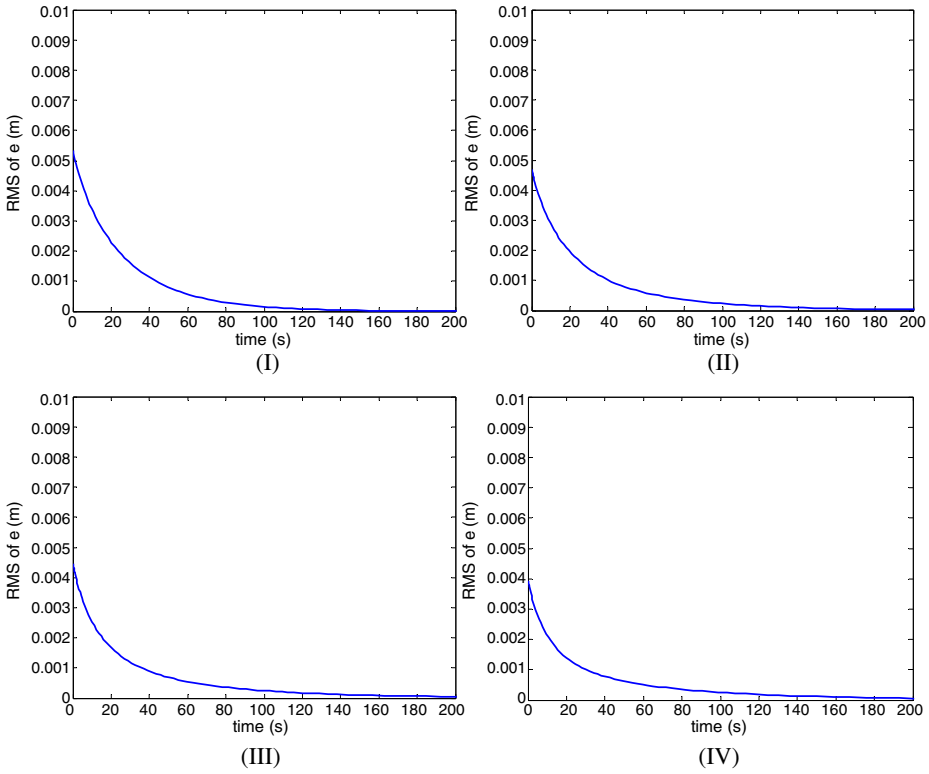

Fig. 10 RMS of shape error, e, for four different cases based on number of actuation points when controlling shape from the *circle* to the *square*: (I) 12, (II) 18, (III) 24, and (IV) 36

15b. This shows their rapid convergence to zero. Comparing the shape errors with and without consideration of robust control for the system with model parameter uncertainties, the robust control method can improve the performance of the system with model parameter uncertainties.

Simulation Set 2: Here we simulate a scenario where a robotic hand handles a deformable object. We consider a case as shown in Fig. 16 where a three-fingered robotic gripper is performing a pick-and-place operation of a soft deformable object, say a dough. We assume that the contact points of the gripper are located at 120° apart. Here we present two different cases. In the first case, the robotic gripper is picking and placing the object without controlling the shape of the object (i.e., the shape controller is turned off). The robotic gripper applies forces on the surface of the object to balance the gravitational force and moves the object to the desired location without controlling the shape of the object. The force applied at each finger tip to balance the gravitational force is given by $f_n = Mg/3\mu$, where, M is the total mass of the object, g is the gravitational acceleration and μ is the coefficient of friction between the object and the robot end-effectors. We choose the mass of the object to be 870 g and the coefficient of friction between the object and the robot end-effectors as 1.6. The normal force at each contact point is calculated as $f_n = 1.78$ N.

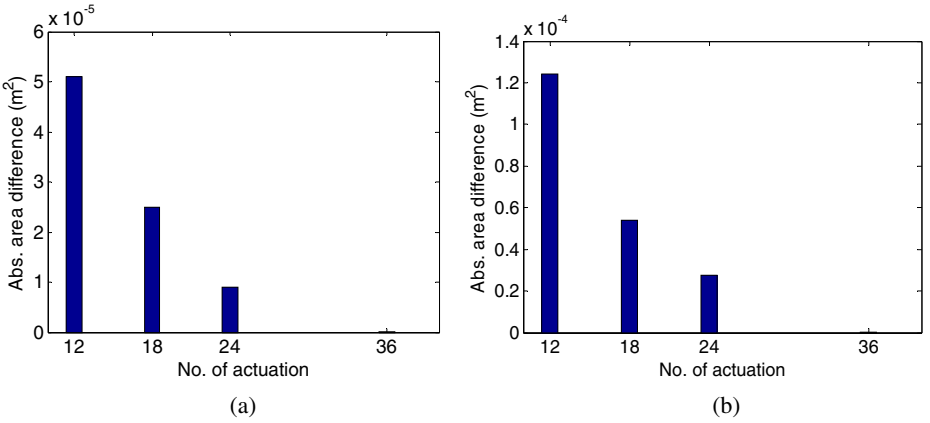

Fig. 11 Absolute area difference between the final shape represented by the boundary points and the desired boundary curve when (**a**) the *circle* is deformed to the *ellipse* and (**b**) when the *circle* is deformed to the *square*

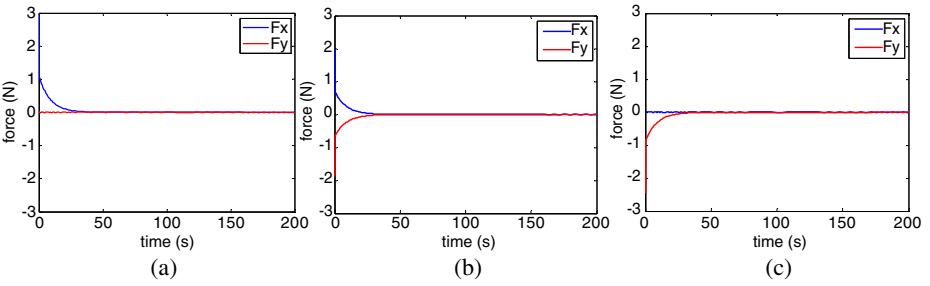

Fig. 12 Contact forces when controlling shape from the *circle* to the *ellipse* for case IV at three contact points located at: (**a**) 0°, (**b**) 50°, and (**c**) 90° with respect to *x*-axis, respectively

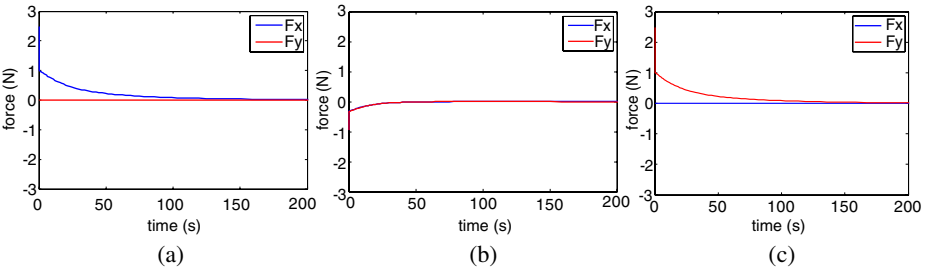

Fig. 13 Contact forces when controlling shape from the *circle* to the *square* for case IV at three contact points located at: (**a**) 0°, (**b**) 50°, and (**c**) 90° with respect to *x*-axis, respectively

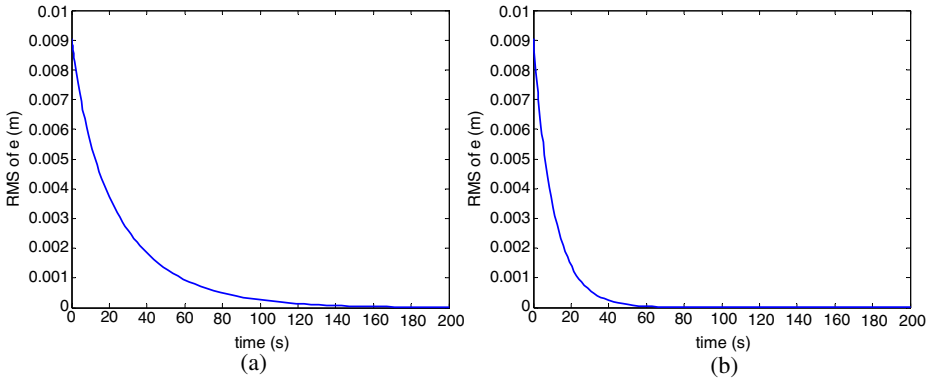

Fig. 14 RMS of shape error, e, when controlling shape from the *circle* to the *ellipse* (**a**) without robust controller and (**b**) with robust controller

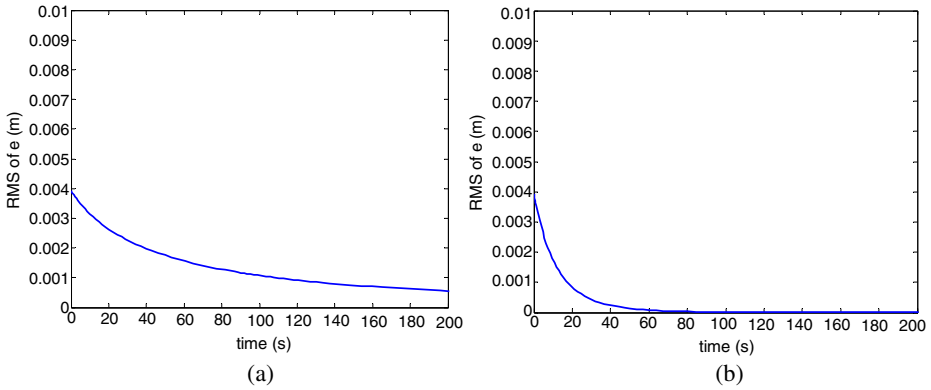

Fig. 15 RMS of shape error, e, when controlling shape from the *circle* to the *square* (**a**) without robust controller and (**b**) with robust controller

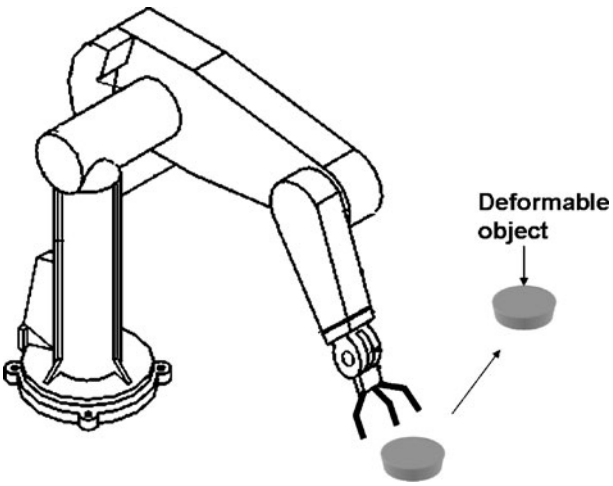

Fig. 16 A robotic gripper is picking and placing a deformable object

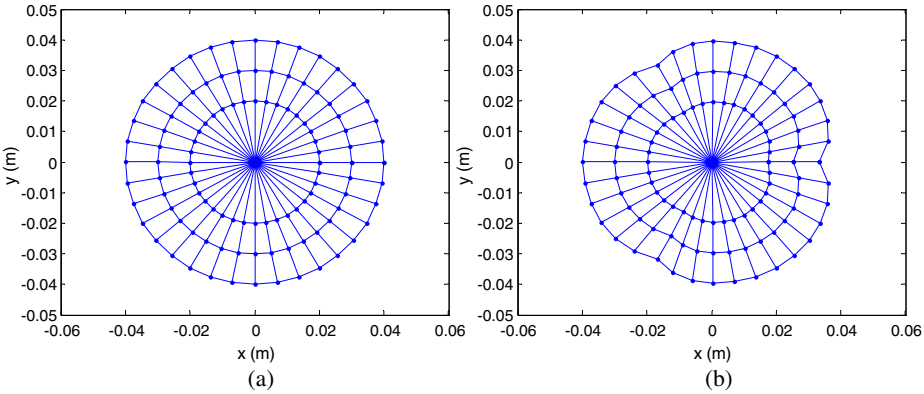

Fig. 17 Pick-and-place operation by a three-fingered robot gripper without the shape controller, (**a**) initial shape of the object, and (**b**) final shape of the object

The dough model is the same as is used in the previous simulation (Set 1). We simulate the above manipulation operation for a duration of 10 s. required to pick-and-place the deformable object. The initial and final shapes of the object are shown in Fig. 17. The shape of the object is not controlled during handling. The RMS of shape error increases as shown in Fig. 19a. In the second case, the robotic gripper performs the same pick-and-place task but with the shape controller turned on. The initial and the final shape of the objects are shown in Fig. 18. The RMS of shape error is shown in Fig. 19b. It is demonstrated by this simulation that the shape of the deformable object can be controlled during manipulation, which in this case, would mean that deformable food products can be manipulated by a robot without distorting their original shapes.

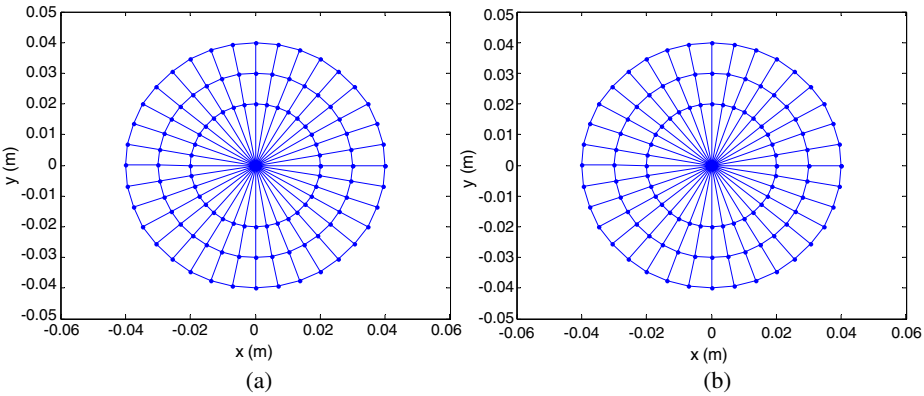

Fig. 18 Pick-and-place operation by a three-fingered robot gripper with shape controller, (**a**) initial shape of the object, and (**b**) final shape of the object

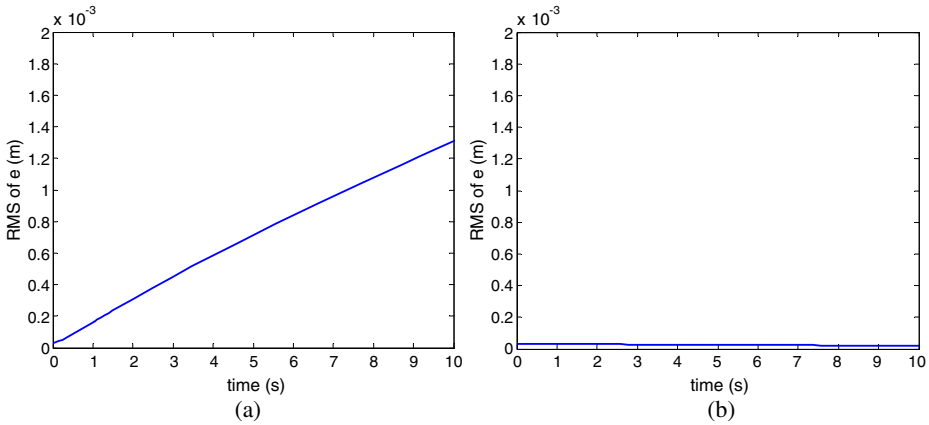

Fig. 19 RMS of shape error, (**a**) when shape control action is turned off, and (**b**) when shape control action is turned on

6 Contributions of this Work and Future Directions

We have developed a new framework to achieve shape control of deformable objects by multiple manipulators. Here the multiple manipulators could be stand-alone manipulators or a gripper with multiple fingers. The methodology presented here describes the modeling techniques of deformable rheological objects subjected to continuous deformation. The integrated dynamics between the rheological object and the multiple manipulators is derived that is used to develop the control law. Using this mathematical model a robust control law is also developed based on robust control theory. To control the shape of the deformable object, a simulation based on a desired planar curve is presented and the boundary is regulated subject to continuous deformation. An optimization-based motion planning scheme for the object is introduced to determine the desired curve parameters on the selected initial contact locations. The planner generates the desired inputs to the system according to the computed desired curve parameters. The motion of each manipulator is controlled independently without communication among them. Further, the robustness of the control system with parameter uncertainty is shown with simulation results.

Future work includes testing the controller with more complex shapes of the deformable object, 3-D objects, and verifying the methodology by experiments. The feasibility of implementing a large number of actuators in real time could be a difficult task. As we model the deformable object as a rheological object having the properties of residual deformation after removing the forces, we are formulating a technique in our future work to use the minimum number of manipulators to control the shape change operations to emulate shape change operation by our fingers while kneading dough to make pizza or pulling a cloth to give a desired shape. Motivated by the work presented in [51] and the reference therein we are investigating how many actuation points and their locations are required to efficiently effect the desired shape change operation.

Appendix: Robustness Analysis

In Section 4, a dynamic shape control approach for deformable object is developed based on the object model without consideration to modeling uncertainties. In practice, modeling uncertainties must be considered for control system designed to interact with deformable objects. In this section, we discuss the robustness of the shape controller with parameter uncertainty. Recalling Eq. 14 with parameter uncertainty, a robust shape controller is developed as

$$\mathbf{u} = \hat{\overline{\mathbf{M}}}\mathbf{v} + \hat{\overline{\mathbf{C}}}\dot{\mathbf{p}} + \hat{\overline{\mathbf{G}}} \tag{21}$$

$$\mathbf{v} = \mathbf{v}_0 + \Delta\mathbf{v} \tag{22}$$

where, $\hat{\overline{\mathbf{M}}}$, $\hat{\overline{\mathbf{C}}}$, and $\hat{\overline{\mathbf{G}}}$ are the estimated or available values of $\overline{\mathbf{M}}$, $\overline{\mathbf{C}}$, and $\overline{\mathbf{G}}$. $\mathbf{v}_0$ is the controller for the nominal system, expressed similarly to Eq. 19 as

$$\mathbf{v}_0 = \mathbf{J}_{\mathbf{M}}^{-1}\left\{-\dot{\mathbf{J}}_{\mathbf{M}}\dot{\mathbf{q}} - \mathrm{K}_p\mathbf{e} - \mathrm{K}_d\dot{\mathbf{e}}\right\} \tag{23}$$

and $\Delta\mathbf{v}$ is the term intended to overcome the effects of modeling uncertainty and is discussed below. Substituting Eq. 21 into Eq. 14 and considering the mass matrix $\overline{\mathbf{M}}$ is a full rank matrix, we get

$$\ddot{\mathbf{p}} = \mathbf{v} + \left(\overline{\mathbf{M}}^{-1}\hat{\overline{\mathbf{M}}} - \mathbf{I}\right)\mathbf{v} + \overline{\mathbf{M}}^{-1}\Delta\overline{\mathbf{C}}\dot{\mathbf{p}} + \overline{\mathbf{M}}^{-1}\Delta\overline{\mathbf{G}} \tag{24}$$

where,

$$\Delta\mathbf{C} = \hat{\overline{\mathbf{C}}} - \overline{\mathbf{C}} \text{ and } \Delta\mathbf{G} = \hat{\overline{\mathbf{G}}} - \overline{\mathbf{G}} \tag{25}$$

In the state space the system becomes,

$$\dot{\mathbf{x}} = \mathbf{A}\mathbf{x} + \mathbf{B}\left\{\mathbf{v} + \left(\overline{\mathbf{M}}^{-1}\hat{\overline{\mathbf{M}}} - \mathbf{I}\right)\mathbf{v} + \overline{\mathbf{M}}^{-1}\Delta\overline{\mathbf{C}}\dot{\mathbf{p}} + \overline{\mathbf{M}}^{-1}\Delta\overline{\mathbf{G}}\right\} \tag{26}$$

where,

$$\mathbf{A} = \begin{bmatrix} \mathbf{0} & \mathbf{I} \\ \mathbf{0} & \mathbf{0} \end{bmatrix},\ \mathbf{B} = \begin{bmatrix} \mathbf{0} \\ \mathbf{I} \end{bmatrix},\ \mathbf{x} = \begin{bmatrix} \mathbf{x}_1 \\ \mathbf{x}_2 \end{bmatrix} = \begin{bmatrix} \mathbf{p} \\ \dot{\mathbf{p}} \end{bmatrix} \tag{27}$$

where, $\mathbf{I}$ is the unit matrix. To analyze the control system stability we define the system error vector as

$$\tilde{\mathbf{e}} = \begin{bmatrix} \mathbf{p} - \mathbf{p}_d \\ \dot{\mathbf{p}} - \dot{\mathbf{p}}_d \end{bmatrix} \tag{28}$$

where $\mathbf{p}_d$ is the desired reference location. The system error equation becomes

$$\dot{\tilde{\mathbf{e}}} = (\mathbf{A} - \mathbf{B}\mathbf{K})\,\tilde{\mathbf{e}} + \mathbf{B}\Delta\mathbf{v} + \mathbf{B}\Delta\phi(\tilde{\mathbf{e}}, t) \tag{29}$$

where,

$$\mathbf{K} = \left[\mathbf{J}_{\mathbf{M}}^{-1}\mathbf{K}_p\ \mathbf{J}_{\mathbf{M}}^{-1}\mathbf{K}_d\right] \tag{30}$$

$$\begin{aligned}\Delta\phi(\tilde{\mathbf{e}}, t) = {} & \left(\mathbf{I} - \overline{\mathbf{M}}^{-1}\hat{\overline{\mathbf{M}}}\right)\mathbf{K}\tilde{\mathbf{e}} + \left(\overline{\mathbf{M}}^{-1}\hat{\overline{\mathbf{M}}} - \mathbf{I}\right)\Delta\mathbf{v} - \overline{\mathbf{M}}^{-1}\hat{\overline{\mathbf{M}}}\mathbf{J}_{\mathbf{M}}^{-1}\dot{\mathbf{J}}_{\mathbf{M}}\dot{\mathbf{q}} \\ & + \overline{\mathbf{M}}^{-1}\Delta\mathbf{C}\dot{\mathbf{p}} + \overline{\mathbf{M}}^{-1}\Delta\mathbf{G}\end{aligned} \tag{31}$$

It is noted that **A**-**BK** is a Hurwitz matrix i.e., all eigenvalues of **A**-**BK** are located in the left half plane. From Lyapunov theory there exist symmetric positive definite matrices $\mathbf{P}_s$ and $\mathbf{Q}_s$ which satisfy the following Lyapunov equation:

$$(\mathbf{A}-\mathbf{BK})^{\mathbf{T}}\mathbf{P_s}+\mathbf{P_s}(\mathbf{A}-\mathbf{BK})=-\mathbf{Q_s} \tag{32}$$

In order to compensate for the effect of model uncertainty, $\Delta\phi(\tilde{\mathbf{e}},t)$, the control signal $\mathbf{\Delta v}$ is designed based on nonlinear robust control theory [52]:

$$\mathbf{\Delta v}=-\frac{\mathbf{B^T P_s}\tilde{\mathbf{e}}\rho(\tilde{\mathbf{e}},t)}{\left\|\mathbf{B^T P_s}\tilde{\mathbf{e}}\right\|\rho(\tilde{\mathbf{e}},t)+\lambda}\rho(\tilde{\mathbf{e}},t) \tag{33}$$

where λ is a positive scalar constant control parameter, $\mathbf{P}_s$ is defined in Eq. 32, and $\rho(\tilde{\mathbf{e}},t)$ is a positive scalar function of the system state which is defined in the following. From the expression of $\Delta\phi(\tilde{\mathbf{e}},t)$, the norm of $\Delta\phi(\tilde{\mathbf{e}},t)$ can be written as

$$\begin{aligned}\|\Delta\phi(\tilde{\mathbf{e}},t)\| &= \left\|\left(\mathbf{I}-\overline{\mathbf{M}}^{-1}\hat{\overline{\mathbf{M}}}\right)\mathbf{K}\right\|\cdot\|\tilde{\mathbf{e}}\|+\left\|\left(\overline{\mathbf{M}}^{-1}\hat{\overline{\mathbf{M}}}-\mathbf{I}\right)\right\|\cdot\|\Delta\mathbf{v}\| \\ &\quad+\left\|\overline{\mathbf{M}}^{-1}\Delta\mathbf{C}\dot{\mathbf{p}}+\overline{\mathbf{M}}^{-1}\Delta\mathbf{G}-\overline{\mathbf{M}}^{-1}\hat{\overline{\mathbf{M}}}\hat{\overline{\mathbf{J}}}_{\mathbf{M}}^{-1}\dot{\mathbf{J}}_{\mathbf{M}}\dot{\mathbf{q}}\right\|\end{aligned} \tag{34}$$

Defining $\|(\mathbf{I}-\overline{\mathbf{M}}^{-1}\hat{\overline{\mathbf{M}}})\mathbf{K}\|=\delta_1(t)$, $\|(\overline{\mathbf{M}}^{-1}\hat{\overline{\mathbf{M}}}-\mathbf{I})\|=\delta_2(t)$, $\|\overline{\mathbf{M}}^{-1}\Delta\mathbf{C}\dot{\mathbf{p}}+\overline{\mathbf{M}}^{-1}\Delta\mathbf{G}-\overline{\mathbf{M}}^{-1}\hat{\overline{\mathbf{M}}}\hat{\overline{\mathbf{J}}}_{\mathbf{M}}^{-1}\dot{\mathbf{J}}_{\mathbf{M}}\dot{\mathbf{q}}\|=\delta_3(t)$, $1-\delta_2(t)>0$, and using Eq. 33, the norm of $\Delta\phi(\tilde{\mathbf{e}},\mathbf{t})$ is obtained as

$$\|\Delta\phi(\tilde{\mathbf{e}},t)\|=\delta_1(t)\|\tilde{\mathbf{e}}\|+\delta_2(t)\rho(\tilde{\mathbf{e}},t)+\delta_3(t):=\rho(\tilde{\mathbf{e}},t) \tag{35}$$

Thus, $\rho(\tilde{\mathbf{e}},t)$ is well defined as

$$\rho(\tilde{\mathbf{e}},t)=(1-\delta_2(t))^{-1}(\delta_1(t)\|\tilde{\mathbf{e}}\|+\delta_3(t)) \tag{36}$$

We now consider the robustness of the shape control system by adding $\mathbf{\Delta v}$ into Eq. 22. The additional control term, $\mathbf{\Delta v}$, is used to overcome the potentially destabilizing effect of the modeling uncertainty $\Delta\phi(\tilde{\mathbf{e}},t)$.

References

1. Erzincanli, F., Sharp, J.M.: Meeting the need for robotic handling of food products. Food Control **8**(4), 185–190 (1997)
2. Denkena, B., Scherger, S.: A concept for shoe last manufacturing in mass customization. CIRP Ann.-Manuf. Technol. **54**(1), 341–344 (2005)
3. Bone, G.M., Capson, D.: Vision-guided fixtureless assembly of automotive components. Robot. Comput.-Integr. Manuf. **19**(1–2), 79–87 (2003)
4. Saadat, M., Nan, P.: Industrial applications of automatic manipulation of flexible materials. Ind. Robot. An Int. J. **29**(5), 434–442 (2002)
5. Henrich, D., Worn, H.: Robot Manipulation of Deformable Objects: Advanced Manufacturing. Springer, New York (2000)
6. Taylor, P.M.: Sensory Robotics for the Handling Of Limp Materials. Springer, New York (1990)
7. Zribi, M., Karkoub, M., Huang, L.: Modelling and control of two robotic manipulators handling a constrained object. Appl. Math. Model. **24**(12), 881–898 (2000)
8. Li, Z., Ge, S.S., Wang, Z.: Robust adaptive control of coordinated multiple mobile manipulators. Mechatronics **18**(5–6), 239–250 (2008)
9. Namvar, M., Aghili, F.: Adaptive force-motion control of coordinated robots interacting with geometrically unknown environments. IEEE Trans. Robot. **21**(4):678–694 (2005)

10. Tokumoto, S., Fujita, Y., Hirai, S.: Deformation modeling of viscoelastic objects for their shape control. In: Proceedings of the 1999 IEEE International Conference on Robotics and Automation, pp. 767–772 (1999)
11. Saha, M., Isto, P.: Manipulation planning for deformable linear objects. IEEE Trans. Robot. 23(6), 1141–1150 (2007)
12. Zhang, Y., Chen, B.K., Liu, X., Sun, Y.: Autonomous robotic pick-and-place of microobjects. IEEE Trans. Robot. **26**(1), 200–207 (2010)
13. Liu, X.Y., Kim, K.Y., Zhang, Y., Sun, Y.: NanoNewton force sensing and control in microrobotic cell manipulation. Int. J. Rob. Res. **28**, 1065–1076 (2009)
14. Kim, K.Y., Liu, X.Y., Zhang, Y., Cheng, J., Wu, S., Sun, Y.: Elastic and viscoelastic characterization of microcapsules for drug delivery using a force-feedback MEMS microgripper. Biomed. Microdevices **11**(2), 421–427 (2009)
15. Pettersson, A., Davis, S., Gray, J.O., Dodd, T.J., Ohlsson, T.: Design of a magnetorheological robot gripper for handling of delicate food products with varying shapes. J. Food Eng. **98**(3), 332–338 (2010)
16. Tavasoli, A., Eghtesad, M., Jafarian, H.: Two-time scale control and observer design for trajectory tracking of two cooperating robot manipulators moving a flexible beam. Robot. Auton. Syst. **57**(2), 212–221 (2009)
17. Tanner, H.G., Kyriakopoulos, J., Krikelis, N.I.: Advanced agricultural robots: kinematics and dynamics of multiple mobile manipulators handling non-rigid material. Comput. Electron. Agric. **31**(1), 91–105 (2001)
18. Sun, D., Liu, Y.H.: Modeling and impedance control of a two-manipulator system handling a flexible beam. ASME J. Dyn. Syst. Meas. Control **119**(4), 736–742 (1997)
19. Sun, D., Mills, J.K., Liu, Y.H.: Position control of robot manipulators manipulating a flexible payload. Int. J. Rob. Res. **18**(3), 319–332 (1999)
20. Liu, Z., Nakamura, T.: Learning the insertion operation of a flexible beam into a hole with a manipulator. Artif. Life Robot. **6**(3), 155–162 (2002)
21. Hirai, S., Wada, T.: Indirect simultaneous positioning of deformable objects with multi pinching fingers based on uncertain model, Robotica. Millenn. Issue Grasp. Manipulat. **18**, 3–11 (2000)
22. Gibson, S.F.F., Mirtich, B.: A Survey of Deformable Modeling in Computer Graphics. MERL Techical Report, TR97-19 (1997)
23. Zhang, Y., Prakash, E.C., Sung, E.: A new physical model with multilayer architecture for facial expression animation using dynamics adaptive mesh. IEEE Trans. Vis. Comput. Graph. **10**(3), 339–352 (2004)
24. Meyer, M., Debunne, G., Desbrun, M., Barr, A.H.: Interactive animation of cloth-like objects in virtual reality. J. Vis. Comput. Animat. **12**(1), 1–12 (2001)
25. Joukhadar, A., Laugier, C.: Dynamic simulation: model, basic algorithms, and optimization. In: Laumond, J.-P., Overmars, M. (eds.) Algorithms for Robotic Motion and Manipulation, pp. 419–434. Peters, Wellesley (1997)
26. Koch, R.M., Gross, M.H., Carls, F.R., Buren, D.F., Von Fankhauser, G., Parish, Y.I.H.: Simulating facial surgery using finite element models. In: ACM SIGGRAPH 96 Conference Proceedings, pp. 421–428 (1996)
27. Pieper, S.D., Laub, D.R., Rosen, J.M.: A finite element facial model for simulating plastic surgery. Plast. Reconstr. Surg. **96**(5), 1100–1105 (1995)
28. Keeve, E., Girod, S., Kikinis, R., Girod, B.: Deformable modeling of facial tissue for craniofacial surgery simulation. Comput. Aided Surg. **3**(5), 228–238 (1999)
29. Kimura, M., Sugiyama, Y., Tomokuni, S., Hirai, S.: Constructing rheologically deformable virtual objects. Proc. IEEE Int. Conf. Robot. Autom. **3**, 3737–3743 (2003)
30. Hu, Y.R., Vukovich, G.: Active robust shape control of flexible structures. Mechatronics **15**(7), 807–820 (2005)
31. Kashiwase, T., Tabata, M., Tsuchiya, K., Akishita, S.: Shape control of flexible structures. J. Intell. Mater. Syst. Struct. **2**(1), 110–125 (1991)
32. Dang, P., Lewis, F.L., Subbarao, K., Stephanou, H.: Shape control of flexible structure using potential field method. In: 17th IEEE International Conference on Control Applications, pp. 540–546. Texas, USA (2008)
33. Faloutsos, P., Panne, M., Terzopoulos, D.: Dynamic free-form deformations for animation synthesis. IEEE Trans. Vis. Comput. Graph. **3**(3), 201–214 (1997)
34. Knopf, G.K., Igwe, P.C.: Deformable mesh for virtual shape sculpting. Robot. Comput.-Integr. Manuf. **21**(4–5), 302–311 (2005)

35. Celniker, G., Gossard, D.: Deformable curve and surface finite elements for free-form shape design. Comput. Graph. (SIGGRAPH'91 Proc) **25**, 257–266 (1991)
36. Rosen, J., Hannaford, B., MacFarlane, M., Sinanan, M.: Force controlled and teleoperated endoscopic grasper for minimally invasive surgery-experimental performance evaluation. IEEE Trans. Biomed. Eng. **46**, 1212–1221 (1999)
37. Kolluru, R., Valavanis, K.P., Smith, S.A., Tsourveloudis, N.: Design fundamentals of a re-configurable robotic gripper system. IEEE Trans. Syst. Man Cybernet.-Part A: Syst. Human. **30**(2), 181–187 (2000)
38. Stone, R.S.W.Brett, P.N.: A flexible pneumatic actuator for gripping soft irregular shaped objects. In: IEEE Colloq. Innov. Actua. Mechatron. Syst., pp. 13/1–13/3 (1995)
39. Seliger, G., Stephan, J.: Handling with ice—the cryo gripper—a new approach. Assem. Autom. **19**, 332–337 (1999)
40. Zhang, D., Lu, G.: Review of shape representation and description techniques. Pattern Recogn. **37**, 1–19 (2004)
41. Loncaric, S.: A survey of shape analysis techniques. Pattern Recogn. **31**(8), 983–1001 (1998)
42. Zhang, D., Lu, G.: Study and evaluation of different Fourier methods for image retrieval. Image Vis. Comput. **23**(1), 33–49 (2005)
43. Kong, X., Luo, Q., Zeng, G., Lee, M.H.: A new shape descriptor based on centroid-radii model and wavelet transform. Opt. Commun. **273**(2), 362–366 (2007)
44. Anelli, M., Cinque, L., Sangineto, E.: Deformation tolerant generalized Hough transform for sketch-based image retrieval in complex scenes. Image Vis. Comput. **25**(11), 1802–1813, (2007)
45. Tarmissi, K., Hamza, A.B.: Information-theoretic hashing of 3D objects using spectral graph theory. Expert Syst. Appl. **36**(5), 9409–9414 (2009)
46. Jain, A.K., Zhong, Y., Jolly, M.P.D.: Deformable template models: a review. Signal Process. **71**(2), 109–129 (1998)
47. Kwan, P.W.H., Kameyama, K., Toraichi, K.: On a relaxation-labelling algorithm for real-time contour-based image similarity retrieval. Image Vis. Comput. **21**(3), 285–294 (2003)
48. Mokhtarian, F., Ung, Y.K., Wang, Z.: Automatic fitting of digitized contours at multiple scales through the curvature scale space technique. Comput. Graph. **29**(6), 961–971 (2005)
49. Du, J.X., Huang, D.S., Wang, X.F., Gu, X.: Shape recognition based on neural networks trained by differential evolution algorithm. Neurocomputing **70**(4–5), 896–903 (2007)
50. Tokumoto, S., Hirai, S., Tanaka, H.: Constructing virtual rheological objects. In: Proc. World Multiconference on Systemics, Cybernetics and informatics, pp. 106–111. Auland (2001)
51. Chen, Y.Q., Moore, K., Song, Z.: Diffusion boundary determination and zone control via mobile actuator-sensor networks (MAS-net)—challenges and opportunities. In: Intelligent Computing: Theory and Applications II, SPIE Defense and Security Symposium, 12–16 April, Orlando, FL,USA (2004)
52. Spong, M.W., Vidyasagar, M.: Robot Dynamics and Control. Wiley, New York (1989)